Investigation of Mechanical Loss Components and Heat Transfer in an Axial-Flux PM Machine

Rafal Wrobel[1], Gyula Vainel[2) 4)], Colin Copeland[3)], Tomasz Duda[3)], Dave Staton[4)] and Phil Mellor[1)]

[1)] Department of Electrical & Electronic Engineering
University of Bristol
Bristol, UK
r.wrobel@bristol.ac.uk

[2)] ThyssenKrupp Presta Hungary Ltd.
Budapest, Hungary
gyula.vainel@thyssenkrupp.com

[3)] Department of Mechanical Engineering
University of Bath
Bath, UK
c.d.copeland@bath.ac.uk

[4)] Motor Design Ltd.
Ellesmere, UK
dave.staton@motor-desig.com

***Abstract*— This paper investigates components of mechanical loss together with heat transfer effects in an axial-flux PM motor. The mechanical loss components generated within electrical machines are well known, however, their prediction or derivation has not been widely reported in the literature. These, together with the electromagnetic loss sources and heat transfer effects are crucial and must be accounted for when considering high-power-density, high-speed and/or compact machine designs.**

This research is focused on separating the mechanical loss components to gain a more in depth understanding of the effects and their importance. Both experimental and theoretical techniques have been employed in the analysis of a machine demonstrator. In particular, hardware tests with dummy rotors have been performed to measure the bearing and windage/drag loss components. These have been supplemented with CFD analysis to theoretically evaluate the aerodynamic effects occurring within the mechanical air-gap accounting for loss and heat transfer.

It has been identified that the analysed hardware demonstrator suffered from bearing loss significantly higher than that suggested by the bearing manufacturer. This has been attributed to design of the mechanical assembly accommodating bearings, which resulted in inappropriate bearing preload. The excessive bearing loss had a significant detrimental effect on the machine thermal behaviour. In contrast, the aerodynamic effects have been found to have less pronounced effects here, due to fully enclosed and naturally cooled machine construction.

Index Terms—Axial-flux PM machine, mechanical loss, heat transfer, computational fluid dynamics, thermal equivalent circuit, bearing loss, windage loss.

I. INTRODUCTION

As developments in materials and manufacturing techniques make less conventional machine constructions feasible, more comprehensive and detailed analysis of prototype machines becomes essential. In that context, a multi-physics and/or multi-disciplinary approach in design-analysis of electrical machines has gained increasing attention [1]-[3], [23]. In addition, the continuous drive towards, compact high-performance and/or cost-effective machine designs imposes further design, manufacture and assembly challenges. These various design and hardware development nuances are difficult to account for without experimentally derived data, which is usually time and resource intensive. Hence, some of the effects might be overlooked in the design process or findings from previous developments need to be adopted approximating particular effect. It is important noting that a machine design that has not been fully informed from analyses and experiments might lead to the performance and/or reliability issues later at the prototyping and testing stage of the machine development process.

One of the essential tasks during the design process of an electrical machine is the derivation of various loss components generated within the machine assembly. The electromagnetic loss sources are well understood and reported in the literature [1]-[3], [23]. In contrast, the mechanical lose components, which are the focus of this investigation, have not been widely discussed by other authors in context of machine design-analysis methodology. In particular, the mechanical loss components associated with the aerodynamic effects, which are difficult to analyse in a timely and generic manner. The existing research in the field is limited to selected aspects of these effects, which are usually considered at the later stages of the design process if found to be significant. The majority of work in the field is devoted to more demanding machine designs with forced air- or liquid- cooling of the rotor or rotor/stator assembly and/or high speed applications [6]-[10], [19]-[24], [41], [42]. The importance of understanding the rotor windage/drag and heat transfer mechanisms has been acknowledged and investigated for various machine designs [6]-[10], [19]-[29], [41], [42].

The bearing loss has received attention in the context of testing techniques and related life span prediction [13]-[17]. There are various types of bearings used in construction of electrical machines. These include the roll bearings, magnetic bearings, air bearings and others [13]-[14]. In this analysis, the most commonly used in electrical machines, the roll bearings are considered only. Existing methods of predicting the bearing loss are based on empirical formulae and do not account for the specifics of the applications in which they were used [13]-[17], [40]. In particular, design of the mechanical assembly accommodating bearings and/or operating conditions, e.g. elevated temperature have a significant impact on bearing performance and generated loss. These effects are difficult to account for at the design stage and tests on machine subassemblies might be required prior to the machine final assembly [14], [15].

This research has been motivated by a number of design-development projects of less conventional and compact machine topologies that the authors have been involved in. In all cases, the mechanical loss had a pronounced, detrimental impact on the machines performance [36]-[38]. This has been later rectified by careful considerations of the mechanical design and assembly processes for the analysed machine designs. In this paper, an axial-flux PM machine prototype has been chosen to illustrate some of the issues related with the mechanical loss derivation and impact of the loss on the machine thermal behaviour.

There are a number of works investigating various aspects of the axial-flux PM machines including the electromagnetic and/or thermal phenomena, which are essential if derivation of the machine operating envelopes is considered [1]–[10]. There has been an upsurge of interest in axial-flux machines due to their potential for greater torque density and more compact construction as compared with their radial-flux counterparts. However, thermal analysis of axial-flux machines is less developed and understood than that of the radial-flux machine topologies. Consequently their thermal behaviour is more challenging to be predicted in an accurate and timely manner [6]-[11]. It is important noting that there have been some developments in predicting thermal behaviour for axial-flux machines. These include mathematical model definition [1]-[9], [12] and detailed analysis of rotor/stator air-gap convective heat transfer phenomena for machine constructions with forced rotor/stator air-gap air cooling [6]-[9], [11]. In this analysis a combination of thermal lumped-parameter equivalent circuit utilising the cuboidal element and computational fluid dynamics (CFD) has been employed to evaluate impact of the mechanical loss on the thermal behaviour of the analysed machine demonstrator. The theoretical analyses have been supplemented with data from tests on the prototype machine.

The research outcomes suggest that the less conventional and compact machine designs, as the analysed hardware demonstrator, require more in depth analysis to understand and identify loss sources including any anomalous effects. In particular, a careful considerations need to be taken when designing mechanical assembly accommodating the bearing set. The assembly needs to provide correct bearing preload and operating environmental conditions, e.g. temperature, to assure and maintain nominal operation of the bearings. Also, the theoretical analysis using the CFD and lumped-parameters equivalent-circuit methods have shown that the excessive bearing loss has significant impact on the machine thermal behaviour and consequently reduced power output capabilities. Moreover, it has been indicated that a high-degree of proficiency/expertise in using these techniques is required to define appropriate models and interpret the calculated results.

This paper is organised in the following manner, the Introduction section outlines the problem of mechanical loss derivation together with the loss impact on the analysed machine thermal behaviour. The Motor Demonstrator section provides selected details regarding construction and operation of the motor demonstrator including the basic motor data. An overview of the mechanical loss components is given in the section Mechanical Loss Components. A description of the experimental setup and testing procedure is included in the Experimental Setup section. The mathematical models used in the analysis are described in the Mathematical Models section. These include the CFD and lumped-parameters equivalent-circuit models. The results are presented and discussed in the Results and Discussion section. The paper concludes with the Conclusion Section.

II. Motor Demonstrator

The research has been focused on a single-sided axial-flux brushless PM motor. The stator core is manufactured using a soft magnetic composite (SMC) with 12 slots (q = 12) and double layer concentrated winding, whereas the rotor assembly includes 10 PM poles (p = 10). The PM poles are segmented and surface mounted on the rotor back iron disc. The rotor is fully enclosed within the motor casing. The stator core together with the winding is encapsulated using high thermal conductivity resin (≈ 1W/m·K) providing good conductive heat transfer into the motor casing. Figs. 1 and 2 illustrate the outline of the motor topology together with a photograph of the prototype. Table I presents basic motor data. The machine is intended to operate with natural air-cooling.

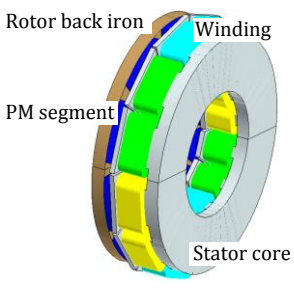

Fig. 1. Outline of the PM axial-flux motor topology

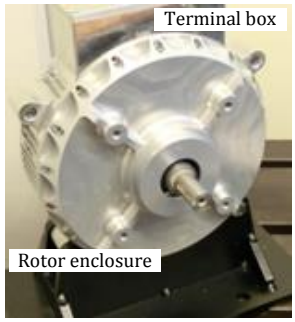

Fig. 2. Prototype motor

Table I. Basic Motor Data

Peak power	14.9kW
Peak torque	70.0Nm
Peak speed	6000rpm
Peak efficiency	> 90.0%
DC link voltage	72.0V
Dimensions	∅237.0mm × 130.0mm

Such a motor construction imposes some challenges regarding heat transfer within the rotor-enclosure. In particular, heat extraction from the rotor assembly is limited due to low air flow/air movement. Furthermore, the mechanical arrangement of the bearings is integrated within the stator assembly, which allows for a compact machine design and cost/time effective manufacture/assembly, but results in an elevated operating temperature of the bearings and potential difficulties with setting and maintaining an appropriate bearing preload. These effects are discussed later in the paper.

III. Mechanical Loss Components

In general, the mechanical power loss generated in electrical machines has two components: bearing loss and aerodynamic loss. The loss components are attributed to contact friction effects in the bearing assembly and to the machine's rotating/moving parts interacting with the surrounding fluid/air respectively.

A. Bearing Power Loss

There are a wide variety of bearing types available which rely upon the rolling action of balls or rollers. In general, a bearing provides a low friction constrained motion from one body relative to another. A typical bearing construction includes five components: inner and outer rings with raceways, rolling elements, cage and seal [13], [14]. The rolling elements are contained between the inner and outer rings providing a connection between the rings with a minimum contact surface area. A cage is used to ensure a uniform distribution of the rolling elements and to prevent their mutual contact. The raceways store a lubricant and prevent axial motion of the elements. A seal is commonly used to contain the lubricant and protect the raceways from contamination.

The bearing loss has two basic loss components attributed to rolling friction and sliding friction. These are caused by various phenomena occurring within the bearing assembly during its operation and include: elastic hysteresis in rolling, sliding due to deformation of contacting elements and/or bearing geometry, spinning of rolling elements, gyroscopic pivotal motion of the rolling elements, sliding between the cage and rolling elements and between the cage and bearing rings, viscous friction due to lubricant motion and seal friction [14]. These fundamental effects are well known, however due to their complexity, they are difficult to quantify. A majority of these phenomena vary during the life span of the bearing, which is caused by the bearing operating conditions/environment, bearing preload, long term bearing wear effects and maintenance schedule, among others. Existing theoretical techniques of predicting bearing loss are based on empirical formulae with several non-deterministic input parameters [14], [40]. Therefore, an experimental approach accounting for the statistical scatter of measured data derived under nominal operating conditions seems to be the most appropriate approach. However, such a method is time and resource intensive and in the case of electrical machines, the bearings must be tested in situ within the machine in order to account for the specific mechanical and preload arrangement of the bearings including any electromagnetic forces. It is important noting that design of the mechanical assembly accommodating bearings has a significant impact on the bearing loss. This might be caused by the non-nominal operating conditions including bearing preload, temperature and others.

B. Windage/Drag Power Loss

The aerodynamic power loss component is frequently referred to as windage loss. In general, this loss component is generated by friction resulting from relative fluid/air movement in reference to the machine's rotating parts, e.g. rotor structure, air-gap, end-windings cooling cavity and internal and external fan assemblies among others. This aerodynamic interaction originates from three fundamental effects that contribute to the overall windage power loss: skin friction, pressure drag and induced drags. These fundamental effects are discussed in detail in many introductory text books in the field, e.g. [30]. However, these effects are difficult to predict individually in a generic and computationally efficient manner. The existing analytical approximations applicable to the design of electrical machines are based on accumulated experience and/or empirically adjusted formulae [24]. These techniques are limited to specific machine topologies and operating conditions. A more widely applicable approach makes use of CFD modelling techniques [6]-[9], [21].

Understanding and accurately predicting this power loss component is particularly important in high-speed and forced air cooled machine designs [6]-[9], [21]. Windage power loss is less significant in more conventional machine designs, however, the thermal aspects of such machine designs are strongly dependent on the aerodynamic effects and resulting heat transfer mechanisms within the motor's air-gap and end-winding cavity [6]-[9], [21]-[24], [41], [42]. There are various correlations available allowing for these heat transfer effects to be accounted for in the design process. The existing correlation techniques require some degree of calibration using experimental data and are limited to a particular class of machine topology and construction. An approach utilising a CFD modelling technique is more generic in that context. However, a degree of calibration is usually required to ensure accuracy and consistency, in particular if less common or more challenging machine design is considered.

IV. Experimental Setup

To assess the mechanical loss together with the aerodynamic and heat transfer effects, two dummy rotors

have been manufactured, see Fig. 3. The dummy rotor with surface protrusions is representative of the surface mounted

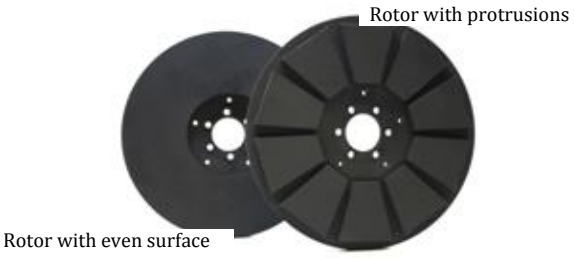

Fig. 3. Dummy rotor assemblies

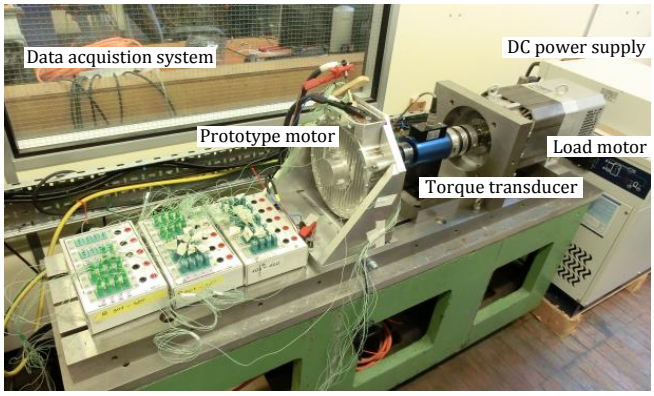

Fig. 4. Experimental setup

PM rotor assembly used in the prototype, whereas the second dummy rotor with a flat, even surface is representative of analytical and experimental studies reported in the literature. Both dummy rotors have been manufactured using non-magnetic and non-electrically conductive material (Tufnol). The machine assembly has been fully instrumented with a number of type-K thermocouples including the inner and outer surfaces of the rotor-enclosure. The test regime included the following rotational tests:

- the bearing loss measurements in isolation have been carried out for the rotor assembly removed from the motor body. An empty machine shaft was rotated at various speeds and bearing temperatures. The bearing temperature was set by exciting the machine windings with DC current and preheating the bearings. The winding phases were connected in parallel to provide uniform winding power loss distribution within the machine body;
- the coupled bearing and windage loss measurements have been performed for the rotor assembly being replaced with the dummy rotors. Similarly as for the previous tests, various rotational speeds and bearing temperatures were considered;
- the DC thermal measurements have been carried out with the dummy rotors. A thermal equilibrium within machine assembly was considered at various winding excitation currents and rotational speeds. In particular, static DC test has been used for initial calibration of the thermal models.

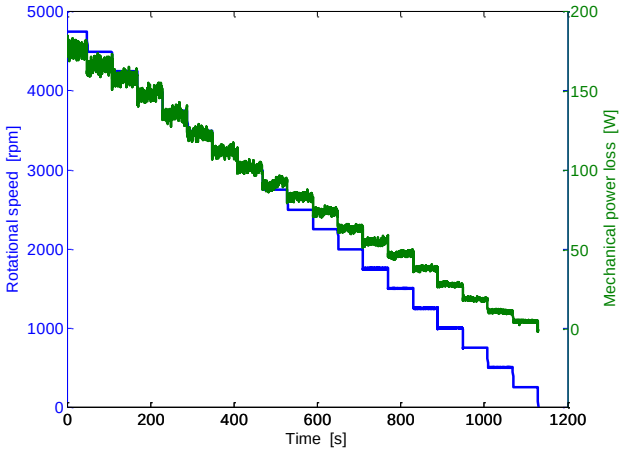

Fig. 5. An example of measured mechanical data loss set

The loss generated or set during the rotational tests are the bearing, windage/drag and DC winding loss only. It is important noting that the tests with dummy rotors do not account for any electromagnetic interaction between the stator and rotor assemblies occurring during motor normal operation. It is expected that in some cases this interaction might lead to further bearing loss due to mechanical forces/ load exerted on the bearing assembly, e.g. axial-force for the axial-flux machine topology [43]. However, this effect is difficult to quantify utilising the existing hardware and is not considered at present.

The experimental setup used in the analysis includes the motor under test, torque transducer and load machine working here as a prime mover, see Fig. 4. The complete list of instruments and components used in the test rig includes: induction machine and industrial drive (Heidenhain QAN200M with Control Techniques SP2402), torque transducer and mechanical data logger (Kistler 4503A50L and CoMo Torque Type 4700), DC power supply (Elektro-Automatik EA-PS 8080-510), electric power measurement setup (Norma 4000 with LEM IT-400S) and temperature logging system (Agilent 34972 with 2×34901A). All the components have been mounted on a custom-built precision finished test bed with locating and aligning features. These are particularly important to avoid erroneous torque readings due to torque offset caused by parasitic loads in the drive train and to provide repeatable measuring conditions when performing several tests with various motor/rotor configurations. It is worth noting that the parasitic loads results mainly from alignment errors in the drive train among other effects.

A single data capture for a particular motor/rotor configuration includes instantaneous torque, rotational speed, mechanical power, temperatures and DC winding power loss where appropriate. These are recorded for the rotational speed increments for both clockwise (CW) and counter clockwise (CCW) rotational direction to compensate for potential torque offset and torque measurement error.

Moreover, a data set containing approximately 600 data points for consecutive rotational speeds is collected over a fixed time interval and used to average the mechanical loss measurements and provide information regarding the measurement uncertainty. Fig. 5 presents an example of a mechanical loss data set from tests on the hardware motor indicating some fluctuations in the measured quantities.

V. Mathematical Models

To demonstrate influence of mechanical loss on thermal behaviour of the analysed machine, thermal analyses employing the computational fluid dynamics (CFD) and lumped-parameter equivalent circuit techniques have been performed. The CFD has been used to derive the windage loss as well as the convective heat transfer within the rotor enclosure. The theoretical findings from CFD have been then used to inform the lumped-parameter model.

A. Computational Fluid Dynamics (CFD)

A three-dimensional (3D) CFD has been employed to evaluate the aerodynamic loss and heat transfer effects. In this analysis, a model definition limiting the solution space to the fluid volume enclosed by the rotor, stator and rotor-enclosure only has been adopted. In addition, due to periodic symmetry, only one tenth of the rotor and rotor-enclosure is represented within the 3D CFD model. Fig. 6 shows the full model domain divided with rotational periodicity as well as the surface mesh of the rotor and shaft. The fluid domain mesh has been created using a fully hexahedral mesh consisting of 1,027,000 cells. Owing to the different turbulent regimes that are expected to exist throughout the speed range, two different turbulence models have been tested, namely, k-ε and shear stress transport (SST). At low rotational speeds, purely laminar models were also created. The non-dimensional first node distance from the wall, namely the y^+ value, was set to below unity.

The SST closure model uses a blended approach to make the best use of the k-ω model in the boundary layer and the k-ε model in the free stream. Owing to the greater accuracy of the k-ω two-equation approach within the boundary layer, the SST model is used for many engineering compressible flows of interest where there are adverse pressure gradients and boundary layer separation [44]. The SST approach has also been shown to be an excellent choice for modelling heat transfer in rotational flows due improved accuracy in predicting boundary layer behaviour [45].

Both the k-ε and SST models have been used by Howey [9] for a very similar application although the authors note little influence of the choice of turbulence model. Airoldi [5] utilizes the k-ε model with enhanced wall treatment approach available in Fluent. Thus, in order to illustrate ambiguities related with CFD model definition in real geometries, both the k-ε and SST models have been used here to present the differences in the predictions.

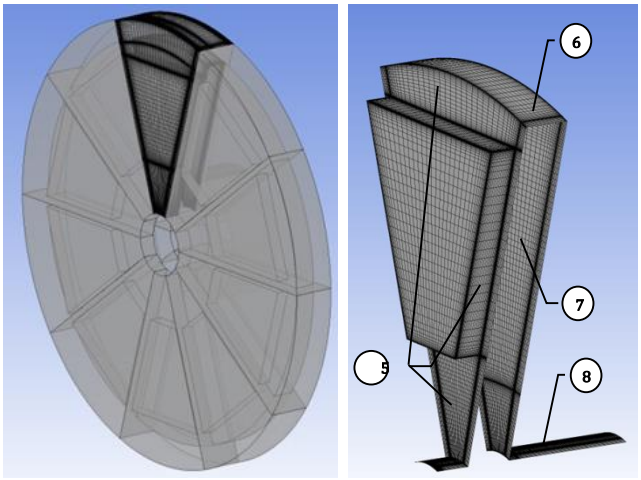

Fig. 6. 3D CFD model representation of the rotor/rotor-enclosure

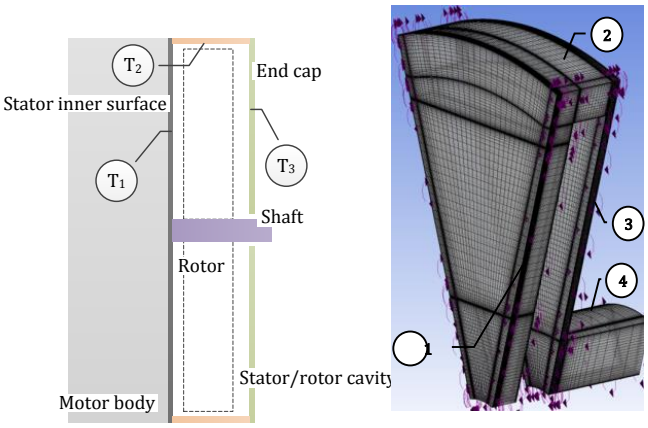

Fig. 7. Cross-section of the motor demonstrator showing the temperature measurements and the corresponding 3D CFD model representation

The boundary conditions were informed by thermocouple temperature measurements made using the experimental setup presented in Fig. 4. Fig. 7 shows the general measurement locations and the corresponding boundary conditions applied to the fluid domain.

Note that since this is a fully enclosed fluid domain, no inlet or exit boundary conditions were required. However, the fluid domain was initialized to standard atmospheric conditions before converging to the final steady-state solution. The stator temperature boundary condition (position 1) was approximated to be a linear radial temperature distribution between two sets of thermocouple measurements located on the stator surface near the end-cap (maximum radius) and hub (minimum radius). The approximation has been informed from initial tests on the machine demonstrator using infrared camera, with the rotor and end-cap assembly removed from the machine body. For the other inner casing surfaces (position 2 and 3 in Fig. 7) a constant average temperature was deemed sufficient. The remaining boundary surfaces were prescribed an adiabatic boundary condition. The model movement was set up with no-slip boundary conditions applied to all surfaces, with the rotor surfaces rotating to match the experimental results.

Note that although most model evaluations where able to reach the convergence criterion of RMS residuals $\leq 10^{-5}$, this target was difficult to reach under some conditions, as will be outlined in the results section.

B. *Lumped Parameters Thermal Model*

A 3D lumped parameter thermal model of the motor demonstrator has been constructed using the cuboidal element approach [12], [34]. Such a model definition allows for the 3D heat transfer, material thermal anisotropy and internal heat generation to be accounted for. It is important noting that definition of the equivalent network has been based on the experimental data from initial tests on the machine demonstrator and the authors' experience/expertise in the field. The equivalent network has a multi-layer structure similar that present in meshed-based modelling techniques and contains all the motor sub-regions/sub-assemblies. These include the winding, stator tooth/slot, stator back iron, rotor PM, rotor back iron, aluminium housing, shaft, bearing assembly and air-gap. The overall number of nodes within the thermal is equal to 250. Due its complexity and volume it is not possible to present the complete thermal network in a single schematic. Figs. 8 and 9 outlines the rotor and housing model representation only, as these are of particular interest in this analysis. Note that the model utilises the circumferential symmetry of the stator assembly, thus a single section of the motor containing a complete stator slot with winding has been analysed here. The rotor model representation shown in Fig. 8 is made up with several cuboidal elements [12] with 3D thermal heat paths accounting for the bearing assembly, air-gap, end-cap and surrounding ambient air. The material thermal data for the machine subregions containing composite materials, e.g. encapsulated winging region, has been derived experimentally using technique outlined in [12]. The material thermal data homogenisation allows for simplified model definition and reduced solution time. The model implementation accounts for the main heat transfer mechanisms occurring in the machine assembly, conduction, convection and radiation where appropriate.

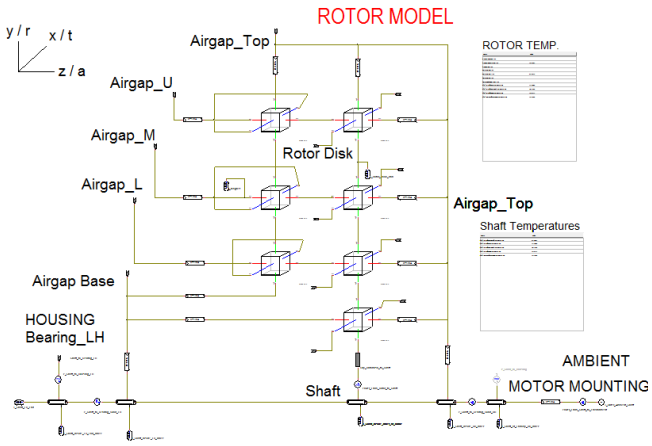

Fig. 8. Thermal model of the rotor assembly

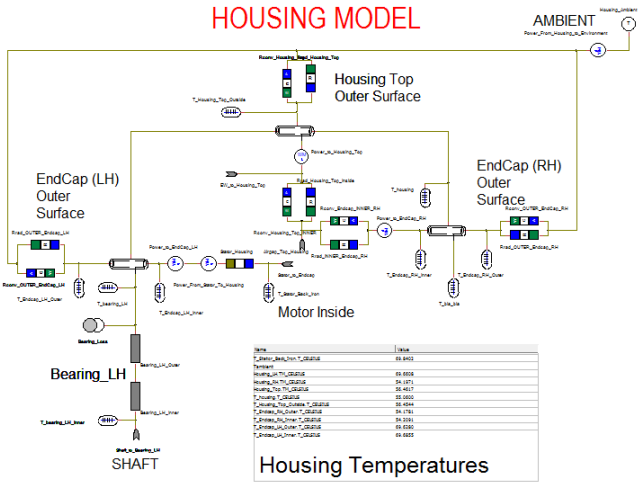

Fig. 9. Thermal model of the housing assembly

Since the stator/winding assembly is encapsulated with high thermal conductivity resin, the conductive heat transfer from the stator/winding assembly into the motor aluminium casing is the major heat transfer mechanism here. However, as the rotor assembly is fully enclosed it is important to account for and understand the convective heat transfer phenomena within the rotor-enclosure. This is particularly important as the elevated rotor temperature has several implications regarding the machine's power output capabilities and reliability.

The model representation of the motor housing is shown in Fig. 9 and accounts for the bearing assembly and related heat paths and the interfacing thermal resistances. The material thermal properties used in the analysis have been derived experimentally or obtained from manufactures data [12]. More detailed information regarding the modelling technique used in application to an axial-flux machine can be found in [38].

VI. Results and Discussion

A series of tests have been carried out to measure the mechanical power loss. Fig. 10 presents the measured bearing loss at different temperatures versus rotational speed. The results suggest relatively high bearing loss when compared to the motor's power output capability. Data provided by the bearing manufacturer suggests bearing loss of 60W at rated speed and nominal operating conditions. It is evident that the measured loss is significantly higher than the expected

bearing loss. As the similar findings have been observed from tests on several prototypes of the axial-flux machine, it has been concluded that design of the mechanical assembly accommodating the bearings is responsible for the elevated/anomalous bearing loss. Here, the bearing mechanical assembly is integrated together with stator/winding making the bearing preload particularly difficult to be set. Also, proximity to the heat source, which is the winding assembly, might have some further implications regarding operation of the bearings. The initial measurements indicate a degree of change in the bearing loss with temperature. This might be attributed to change of properties for the bearing lubricant at elevated temperature, and bearing assembly thermal expansion among others. However, more generic observations and statements regarding thermal dependence of the bearing loss are difficult to make based on this limited data. An experimental approach accounting for the statistical distribution of the data and a wider range of temperatures would be more appropriate, however, this might not be

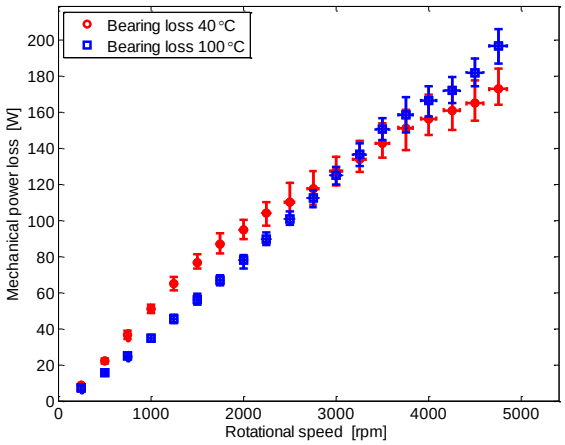

Fig. 10. Measured bearing power loss versus rotational speed

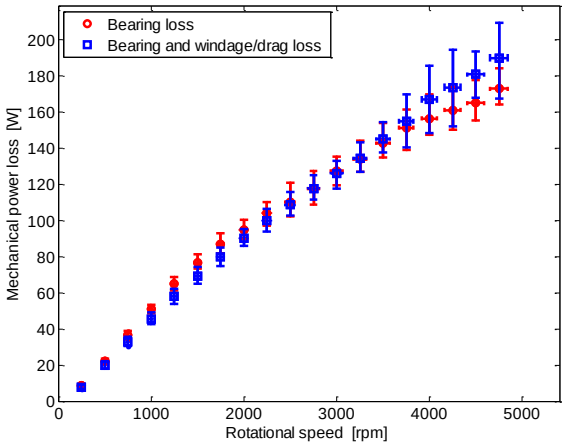

Fig. 11. Measured mechanical power loss versus rotational speed

feasible if a standard evaluation procedure of a prototype machine is used, as is the case in this analysis.

In the experiment, the bearing assembly temperature was set by energising the stator wingding with DC excitation and adjusting it to achieve the required temperature. Here, two test points, 40^0C and 100^0C were analysed. The rotor assembly has been removed from the motor body prior to the tests. It is important to note that in the analysed motor demonstrator a set of two sealed ball bearings, deep groove radial and angular contact were used. In particular, the angular contact bearing was used to transfer the axial load resulting from interaction between stator and rotor assemblies.

Initial tests on the dummy rotor disc with smooth surfaces indicated no discernible increase in loss. Thus only results are presented for the dummy rotor with protrusions.

Fig. 11 shows measured mechanical loss data from tests with this dummy rotor emulating the original rotor assembly. These results have been compared against the bearing loss data from previous tests. Both data sets correspond to the same bearing temperature, here 40^0C. When analysing the measured data, some increase in mechanical loss at higher speeds is evident. This may be attributed to the windage loss. It would be expected that the combined bearing and windage loss is higher than the bearing loss only, across the analysed speed range. However, the results suggest that at lower speeds the loss from bearing only is higher than the combined bearings and windage loss. This may be related here to the measurement uncertainties.

Note that mechanical torque associated with the mechanical power loss is usually orders of magnitude lower than that generated at normal operation of the motor. The typical class of accuracy for the torque transducers is 0.1, which translates to the measurement error within ±0.1% of the rated/nominal torque. It is, therefore, important to make sure that accuracy of the measuring system and fidelity of the experimental setup is sufficient for measurement of the mechanical loss components. In the experimental setup used the nominal torque error was ±0.05Nm. As the measured mechanical power is a product of torque and angular speed the accuracy of the speed measurement is also important. Here, the rotational speed measurement error is ±2%. The overall nominal measurement error for the power measurement can be found from the error propagation theorem. It is important noting that uncertainty of the speed measurement is also affected by accuracy of the speed control for the prime mover. To give some insight into the measurement uncertainty for the analysed motor, the averaged power loss data shown in Figs. 10 and 11 has been supplemented with the error bars. The measurement uncertainty has been derived from statistical analysis/spread of the measured data points.

The temperature measurement uncertainty is attributed to the thermocouple type used as well as temperature range over which the measurements were taken. Here, type-K thermocouples were used with measurement error of ±1.5^{0}C

for the analysed temperature range. To improve the temperature measurement uncertainty attributed to anomalous readings, multiple thermocouples for the equivalent machine subassemblies/subregions were used, and the measured data was appropriately averaged.

Table II. Rotational Reynolds Number

G (g/R) – magnet/stator		**0.0156**
G (g/R) – back side rotor/stator		**0.0260**
RPM	**Ang. velocity (rad/s)**	**Rotational Reynolds No. (Re_θ)**
500	52.40	3.31×10^4
1500	157.10	9.92×10^4
2500	261.80	1.65×10^5
3500	366.50	2.31×10^5
4500	471.20	2.97×10^5

When inspecting the measured results accounting for the measurement uncertainty it is evident that the experimental approach of separating the mechanical loss components might not yield the expected resolution/accuracy as is the case in the analysed motor. This is particularly prominent when one of the mechanical loss components dominates. Here, the bearing related loss is significantly higher than the aerodynamic loss.

To have a more in-depth insight into the aerodynamic loss, a series of CFD analyses have been performed. In order to embark on a CFD study of a rotating fluid cavity, it is important to establish whether the fluid is laminar, turbulent, or a transitional phase between the two regimes. This is most often assessed using two non-dimensional parameters, the ratio of the stator-rotor gap and the tip radius ($G = g/R$) and the rotational Reynolds number ($Re_\theta = \omega R^2/\nu$), where ω is the angular velocity in rad/s and ν is the kinematic viscosity of ambient air. These calculations are provided in Table II. It is important to note that the values of the G ratio and rotational Reynolds number listed in Table II both utilize the rotor back iron radius.

The authors that have studied transition in annular rotor stator cavities do not identify a clear transition from laminar to turbulent flows, in part due to the complexity of the instabilities that can develop. Four flow regimes have been proposed by Daily and Nece [32] where for G ≈ 0.012, a merged boundary layer transitions from laminar to turbulent $Re_\theta \approx 4.0\times10^4$. At G ≈ 0.025, the transition occurs at $Re_\theta \approx 1.0\times10^5$. Schouveiler et al. [31] describes a more complex series of turbuent instabilities that can appear as low as $Re_\theta \approx 6.0\times10^4$ for G = 0.02.

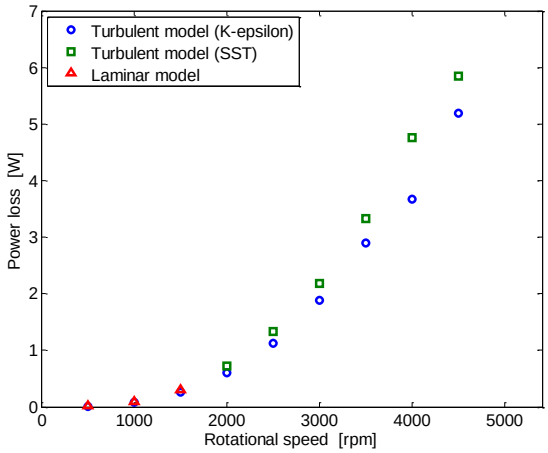

Fig. 12. CFD prediction of windage/drag loss

However, Howey et al. [8], [9] suggests a transition to turbulent flow for $Re_\theta \approx 3.0\times10^5$ for G ≈ 0.01. This highlights one of the most significant hindrances to attempting to model an axial-flux machine in CFD. If the transition from laminar to turbulent for 0.015 < G < 0.025 could be in the range between $4.0\times10^4 < Re_\theta < 3.0\times10^5$, this covers most of the operating range in Table II. This can be very problematic since, as described in [33], the existing turbulent transition closure models can be unstable, and computationally expensive. Moreover, it is very difficult to experimentally validate transition predictions without complex experimental setups.

The approach employed here is to provide data for two different turbulence models (K-epsilon and SST) from 2000rpm - 4500rpm, and laminar solutions from 500rpm - 1500rpm. This assumes an abrupt laminar to turbulent transition at $Re_\theta \approx 1.0\times10^5$ which is in keeping with many of the literature sources. Fig. 12 provides the windage/drag power loss results from the CFD simulation as a function of rotational speed. As noted above, the data is populated by a laminar model from 500rpm-1500rpm and two turbulence models between 2000rpm-4500rpm. In addition, the K-epsilon turbulence model was tested below 2000rpm to understand the sensitivity of the prediction to the assumption of transition. When analysing results from the CFD analysis, similar trends of the windage/drag power loss have been observed for the adopted models. It has been shown that the windage/drag loss generated within the analysed motor assembly is relatively minor compared to the bearing loss thus confirming earlier results from tests on the motor demonstrator.

The local stator convective heat transfer coefficient is defined as the quotient resulting from dividing the local heat flux density $q(r;\theta)$ by the temperature difference between the stator wall and the local bulk fluid temperature (1). However as indicated by Howey [39], owing to the difficulty in measuring the local stator gap temperature, it is commonplace to replace it with an arbitrarily defined

reference temperature. The most common approach is to use the air inlet or ambient temperatures [39].

$$h_{stator} = \frac{q(r,\theta)}{T_{stat.-wall}(r,\theta) - T_{ref}} \quad (1)$$

Figs. 13 and 14 provide a comparison of the distribution of the local stator heat transfer coefficient using two volume-averaged definitions of reference temperatures. The differences in absolute values illustrates that this coefficient strongly depends on the definition of the reference temperature.

Moreover, since this coefficient is important in defining the relationship between stator heat flux and the temperature gradient across the air gap in models such as that shown in Fig. 8, the use of an arbitrary ambient reference condition is not ideal. This is especially the case in a closed rotor design where there is no significant circulation of cool air.

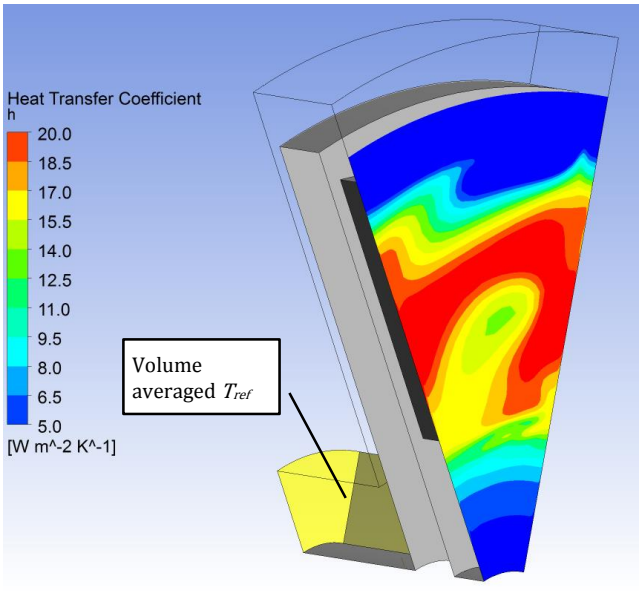

Fig. 13. Local heat transfer coefficient defined using a constant reference temperature taken from the rotor shaft cavity (SST - 4500rpm)

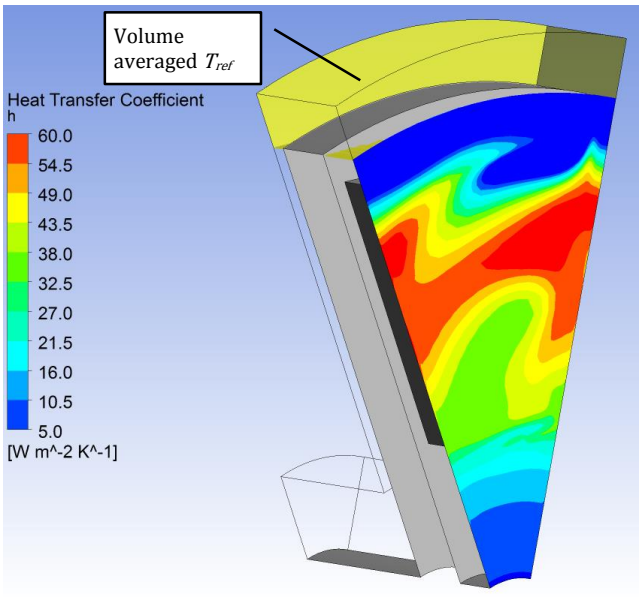

Fig. 14. Local heat transfer coefficient defined using a constant reference temperature taken from the rotor enclosure (SST- 4500rpm)

With this in mind, Fig. 15 shows the air-gap convective heat transfer coefficient predicted from the CFD model using a volume-averaged air gap temperature as the reference condition. Unlike the windage loss, the prediction of convection heat transfer show significant discrepancy between the two turbulent models. In particular, the K-epsilon model suggests significantly higher convective heat transfer effects than the SST and laminar models. This illustrates the importance of using caution in treating CFD simulations as a substitute for experimentally derived values. Considering the motor construction where the rotor protrusions shown in Figure 3 create gaps where separation and a upward flowing vortex is formed [9], the results from the SST model ought to be more representative of the phenomena occurring within the hardware demonstrator. This is also reflected by the experience expressed by other authors [44, 45, 33].

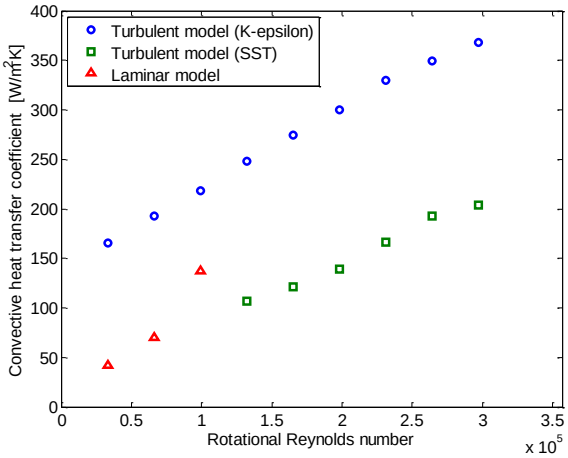

Fig. 15. Convective heat transfer coefficient versus rotational Reynolds number

It is also useful to note from Figs. 13 and 14 that the convective heat transfer coefficient varies radially and circumferentially across the rotor-stator air-gap. However, this map relies on a fixed definition of reference temperature. As explained by Howey [39], the most appropriate definition of reference temperature (1) is the local bulk stator air-gap fluid temperature. Airoldi et al. [5] used the temperature at the centre of the running clearance ($T_{mid-gap}$) to generate the following definition of the local heat transfer coefficient:

$$h_{stator} = \frac{q(r,\theta)}{T_{stat.-wall}(r,\theta) - T_{mid-gap}(r,\theta)} \quad (2)$$

This definition is used to study the heat transfer distribution and the influence of rotor speed using the three radial distributions shown in Fig. 16.

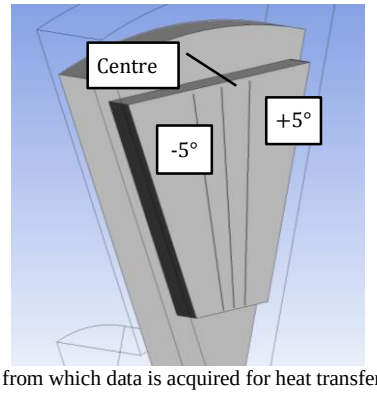

Fig. 16. Lines from which data is acquired for heat transfer calculation

The calculated distribution of local heat transfer coefficient is shown in Fig. 17 for three different rotor speeds: 1000rpm, 2500rpm and 4500rpm. In addition the circumferential distribution is also demonstrated with radial distributions ± 5° from the centreline. These results indicate that some regions of the rotor/stator assembly located within the rotor enclosure exhibit improved convective heat transfer as compared with other parts. In particular, the region located near the outer periphery of the rotor is exposed to higher air velocity resulting in improved convective heat transfer. It is expected that in some cases, where variation of the convective heat transfer within the air gap is more severe, localised stator/rotor hot spots might arise.

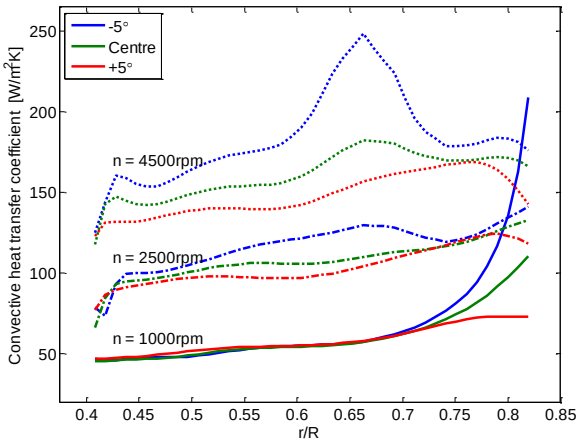

Fig. 17. Radial distribution of the local heat transfer coefficient at 1000rpm, 2500rpm and 4500rpm using the SST turbulence model

While the distribution is useful, it is current common practise when analysing the convective heat transfer to use an averaged value of the convective heat transfer coefficient as given in Fig. 15. The averaged coefficient allows for a simple comparison between various operating conditions of the analysed motor and can be used to inform a non-CFD thermal model, e.g. the lumped parameter thermal model discussed earlier. What is clear, however, from this work is that the definition of the reference temperature used in the local mean heat transfer coefficient (1) ought to be in keeping with the lumped parameter thermal model setup. That is, if the value of the heat transfer coefficient is used in the circuit connecting the stator wall to the local fluid gap properties, using an ambient reference temperature in the definition of the convective coefficient is not advisable.

The equivalent circuit thermal model of the machine demonstrator has been calibrated with data from DC thermal tests as it has been outlined earlier. An initial sensitivity analysis has been performed using the thermal model to identify the main heat transfer paths and mechanisms together with construction/assembly nuances, which have a significant

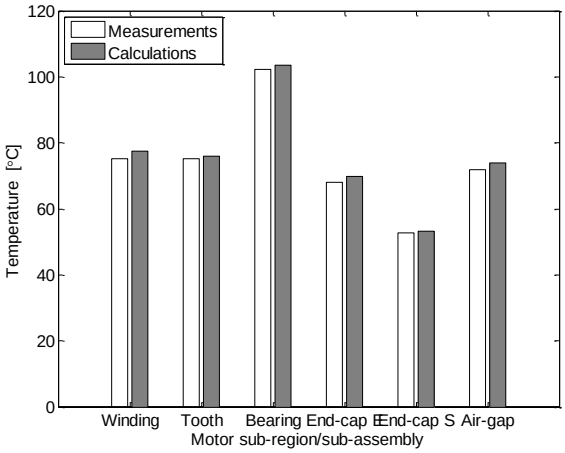

Fig. 18. Measured and calculated temperatures within selected motor sub-regions/sub-assemblies at n = 4500rpm $P_{electrical}$ = 88W, $P_{mechanical}$ = 162W

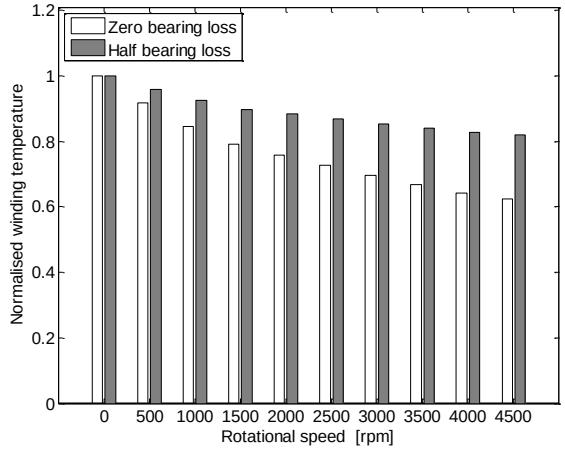

Fig. 19. Normalised winding temperature versus rotational speed for various bearing loss levels

impact on the motor thermal behaviour. The analysis confirmed that the main heat transfer path is provided by conduction from the impregnated stator/winding assembly to the motor housing. As this is the intended mechanism for evacuating heat from the machine body, correct calibration of any interface thermal resistances from the stator/winding to the motor casing were found to be crucial to the accuracy of the thermal model. The calibrated model is the basis for the analysis of the convective heat transfer effects within the motor air-gap/rotor-enclosure.

Fig. 18 presents averaged measured and calculated temperatures within the motor sub-regions/sub-assemblies. A single test point is shown only for the results clarity. Here, the rotational speed is n = 4500rpm, electrical power loss within the motor winding $P_{electrical}$ = 88W for DC excitation and mechanical power loss is $P_{mechanical}$ = 162W. As would be expected, considering calibrated model, good correlation between the measured and calculated data is demonstrated. Also, it is worth mentioning that the close data correlation has been found across entire range of the excitation currents and rotational speeds considered in this analysis. That demonstrates efficacy of the proposed model. Also, the calibrated equivalent circuit thermal model allows for analysis of various effects within the machine assembly to be performed in a timely manner. Here, to give some insight into the heat transfer phenomena within the motor air-gap/rotor-enclosure a supplementary sensitivity analysis has been carried out. Initially a low value of convective heat transfer representative of the locked/stationary rotor test has been used, 10W/m^{2}K -25W/m^{2}K, and later a CFD predicted heat transfer coefficient has been introduced. To illustrate, an increase of the heat transfer coefficient to the maximum predicted value, 376W/m^{2}K, only resulted in a 3% temperature drop for the winding. This confirms that the conductive heat transfer mechanism dominates in the stator/winding assembly. In this analysis, the electromagnetic loss components generated within the machine assembly, including the PM rotor, at normal operation has not been considered. However, it is expected that the combined effects of the generated rotor loss and heat dissipation from the rotor will have a pronounced impact on the overall machine performance. In particular, the machine power output reduction at higher speed operation is expected due to elevated PM temperature as consequence of increase in generated PM rotor loss and deterioration of PM material properties with temperature. These phenomena will be investigated in the future work.

To evaluate the severity and demonstrate the importance of the mechanical loss/bearing loss in the analysed motor prototype, a series of thermal analyses have been carried out for various bearing loss levels. Two case scenarios have been assumed here, zero bearing power loss and half of the original bearing loss. Predictions of the winding temperature from these analyses have been compared against the original data where the complete bearing loss is accounted for. Fig. 19 presents the normalised winding temperature indicating a significant reduction of the winding temperature at higher speed for both analysed case scenarios. This confirms the importance of the mechanical/bearing loss components in the design/analysis of the compact/high-performance electrical machines.

VII. Conclusions

Mechanical power loss has a significant impact on a motor performance, yet very little information regarding this issue exists in the literature. An overview of the problem has been given together with an illustration of the effects on a compact single sided axial-flux PM machine. It has been identified that the analysed hardware demonstrator suffered from excessive bearing loss. This has been attributed to the mechanical assembly accommodating bearings and resulting from excessive preload imposed on the bearing set. The measured data suggests three time increase of the bearing loss as compared with the manufacturer provided data. Note that the manufacturer data assumes nominal operating conditions

for the bearings. These indicate importance of the mechanical design in overall machine design. A simple assumption regarding the bearing loss based on a data sheet might be inadequate and a testing procedure accounting for the anomalous mechanical loss needs to be considered. Also, it has been shown that the elevated bearing loss had a detrimental effect on the machine thermal behaviour and consequently power output capability. The theoretical findings suggest that reduction of the anomalous bearing loss for the analysed machine leads to significant decrease of winding temperature at higher speeds, e.g. reducing the anomalous bearing loss by a half decreases the winding temperature by 20%. In contrast, the aerodynamic effects have been found to have less pronounced effects here, due to fully enclosed and naturally cooled machine construction. Majority of the loss generated within the encapsulated stator/winding assembly is dissipated by conductive heat transfer into the motor casing.

Furthermore, the complexity of the mechanical loss derivation has been outlined. A test procedure on a motor demonstrator has been described in detail. The approach utilises tests on the motor sub-assemblies to identify and quantify contribution of the mechanical loss components. In particular, tests with dummy rotors have been performed to separate the mechanical losses and provide some insight into the convective heat transfer within the rotor/rotor enclosure assembly. Some limitations of the experimental approach for separating the mechanical loss components have been discussed, particularly the measurement uncertainties attributed to the experimental setup and measuring instruments used. The experimental activities have been supplemented with CFD and equivalent circuit thermal analyses to give some insight into the mechanical and heat transfer effects related to the rotor sub-assembly. Some details regarding model definition/application of the theoretical techniques employed in the research have been given. Limitations and uncertainties attributed with the theoretical methods used were also illustrated and discussed. These are particularly important in context of multi-physics and multi-disciplinary machine design-analysis, where more informed design methodology is required.

VIII. REFERENCES

[1] F. Marignetti, V. Delli Colli, Y. Coia, "Design of Axial Flux PM Synchronous Machines Through 3-D Coupled Electromagnetic Thermal and Fluid-Dynamical Finite-Element Analysis," *IEEE Transactions on Industrial Electronics*, vol. 55, no. 10, pp. 3591– 3601, October 2008.

[2] S. Scowby, R. Dobson, M. Kamper, "Thermal Modelling of an Axial Flux Permanent Magnet Machine," *Applied Thermal Engineering*, vol. 24, no. 2, pp. 193 – 207, February 2004.

[3] R. Wang, M. Kamper, R. Dobson, "Development of a Thermofluid Model for Axial Field Permanent-Magnet Machines," *Transactions on Energy Conversion, IEEE*, vol. 20, no. 1, pp. 80–87, March 2005.

[4] C. Lim, J. Bumby, R. Dominy, G. Ingram, K. Mahkamov, N. Brown, A. Mebarki, M. Shanel, "2-d Lumped-Parameter Thermal Modelling of Axial Flux Permanent Magnet Generator," *Proceedings of the 2008 International Conference on Electrical Machines (ICEM 2008)*, pp. 1 – 6, September 2008.

[5] G. Airoldi, G. Ingram, K. Mahkamov, J. Bumby, R. Dominy, N. Brown, A. Mebarki, and M. Shanel, "Computations on Heat Transfer in Axial Flux Permament Magnet Machines," *Proceedings of the 2008 International Conference on Electrical Machines (ICEM 2008)*, pp. 1 – 6, September 2008.

[6] D. A. Howey, P. R. N. Childs, A. S. Holmes, "Air-Gap Convection in Rotating Machines," *IEEE Transactions on Industrial Electronics*, vol. 59, no. 3, pp. 1367 – 1375, March 2012.

[7] R. Camillieri, D. A. Howey, M. D. McCulloch, "Thermal Limitations in Air-Cooled Axial Flux In-Wheel Motors for Urban Mobility Vehicles: a Preliminary Analysis," *Conference on Electrical Systems for Aircraft, Railway and Ship Propulsion (ESARS 2012)*, pp. 1 – 8, October 2012.

[8] D. A. Howey, A. S. Holmes, K. R. Pullen, "Measurement and CFD Prediction of Heat Transfer in Air-Cooled Disc-Type Electrcal Machines," *IEEE Transactions on Industry Applications*, vol. 47, no. 4, pp. 1716 – 1723, August 2011.

[9] D. A. Howey, A. S. Holmes, K. R. Pullen, "Measurement of Stator Heat Transfer in Air-Cooled Axial Flux Permanent Magnet Machines," *35th IEEE Industrial Electronics Annual Conference (IECON 2009)*, pp. 1197 – 1202, November 2009.

[10] A. C. Malloy, R. F. Martinez-Botas, M. Jaensch, M. Lamperth "Measurement of Heat Generation Rate in Permanent Magnet Rotating Electrical Machines," *6th IET International Conference on Power Electronics, Machines and Drives (PEMD 2012)*, pp. 1 – 6, March 2012.

[11] D. Staton, A. Cavagnino, "Convection heat transfer and flow calculations suitable for electric machines thermal models," *IEEE Transactions on Industrial Electronics*, vol. 55, no. 10, pp. 3509 –3516, October 2008.

[12] R. Wrobel, P. H. Mellor, "A General Cuboidal Element for Three-Dimensional Thermal Modelling," *IEEE Transactions on Magnetics*, vol. 46, no. 8, pp. 3197 – 3200, August 2010.

[13] T. Synnot, "Mechanical Aspects of High Performance Electrical Machines – Hybrid Bearings for Integral Motors," *UK Magnetics Society One Day Seminar*, pp. 1-3, February 2013.

[14] T. A. Harris, M. N. Kotzalas, "Advanced Concepts of Bearing Technology – Rolling Bearing Analysis," *Taylor & Francis Group, CRC Press Book*, 2007.

[15] M. Calasan, M. Ostojic, D. Petrovic, "The retardation Method for Bearing Loss determination," *International Symposium on Power Electronics, Electrical Drives, Automation and Motion, (SPEEDAM 2012)*, pp. 25–29, June 2012.

[16] S. Marble, B. P. Morton, "Predicting the Remaining Life of Propulsion System Bearings," *IEEE Aerospace Conference*, pp. 1–8, March 2006.

[17] I. D. Ilina, "Experimental Determination of Moment of Inertia and Mechanical Loss vs. Speed, in Electrical Machines," *7th International Symposium on Advanced in Electrical Engineering, (ATEE 2011)*, pp. 1-4, May 2011.

[18] W. K. S. Khoo, K. Kalita, S. D. Garvey, "Practical Implementation of the Bridge Configured Winding for Producing Controllable Transverse Forces in Electrical Machines," *IEEE Transactions on Magnetics*, vol. 47, no. 6, pp. 1712-1718, June 2011.

[19] H-P. Liu, M. D. Werst, J. J. Hahne, D. Bogard, "Investigation of Windage Splits in an Enclosed Test Fixture Having a High-Speed Composite Rotor in Low Air Pressure Environments," *IEEE Transactions on Magnetics*, vol. 41, no. 1, pp. 316-321, January 2005.

[20] H-P. Liu, M. D. Werst, J. J. Hahne, D. Bogard, "Splits of Windage Losses in Integrated Transient Rotor and Stator Thermal Analysis of a High-Speed Alternator During Multiple Discharges," *IEEE Transactions on Magnetics*, vol. 41, no. 1, pp. 311-315, January 2005.

[21] P. H. Connor, S. J. Pickering, C. Gerada, C. N. Eastwick, C. Micallef, "CFD Modelling of an Entire Synchronous Generator for Improved Thermal Management," *6th IET International Conference Power*

Electronics, Machines and Drives, (PEMD 2012), pp. 1-6, March 2012.
[22] H. Hofmann, S. R. Sanders, "High-Speed Synchronous Reluctance Machine with Minimized Rotor Losses," *IEEE Transactions on Industry Applications*, vol. 36, no. 2, pp. 531–539, March/April 2000.
[23] G. J. Atkinson, B. C. Mecrow, A. G. Jack, D. J. Atkinson, P. Sangha, M. Benarous, "The Analysis of Loss in High-Power Fault-Tolerant Machines for Aerospace Applications," *IEEE Transactions on Industry Applications*, vol. 42, no. 5, pp. 1162–1170, September/October 2006.
[24] J. E. Vranick, "Prediction of Windage Power Loss in Alternators," *NASA Technical Note*, TN D-4849, pp. 1 – 18, October 1968.
[25] R. F. Handschuh, M. J. Hurrell, "Initial Experiments of High-Speed Drive System Windage Losses," *NASA Technical Note*, TM-2011-216925, pp. 1 – 17, November 2011.
[26] M. Saint Raymond, M. E. Kasarda, P. E. Allaire, "Windage Power Loss Modeling of a Smooth Rotor Supported by Homopolar Active Magnetic Bearings," *Journal of Tribology*, vol. 130, no. 2, pp. 1 – 8, September 2007.
[27] M. J. Hill, R. F. Kunz, R. B. Medvitz, R. F. Handschuh, L. N. Long, R. W. Noack, P. J. Morris, "CFD Analysis of Gear Windage Losses: Validation and Parametric Aerodynamic Studies," *Journal of Fluids Engineering*, vol. 133, no. 3, pp. 1 – 10, March 2011.
[28] R H. Jansen, T. P. Dever, "G2 Flywheel Module Design," NASA Technical Note, CR-2006-213862, pp. 1 – 20, August 2006.
[29] F. Chaari, M. Ben Romdhane, W. Baccar, T. Fakhfakh, M. Haddar, "Windage Power Loss in Spur Gear Sets," WSEAS Transactions on Applied and Theoretical Mechanics, vol. 7, no. 2, pp. 159 – 168, April 2012.
[30] G. K. Batchelor, "An Introduction to Fluid Dynamics," Cambridge University Press, 2005.
[31] L. Schouveiler, P. Le Gal, and MP Chauve. "Instabilities of the flow between a rotating and a stationary disk" *Journal of Fluid Mechanics*, vol. 443, pp. 329 – 350, 2001.
[32] J.W. Daily and R.E. Nece. "Chamber dimension effects on induced flow and frictional resistance of enclosed rotating disks" *ASME J. Basic Eng*, vol. 82, no. 1, pp. 217 – 232, 1960.
[33] D. Howey. "Thermal Design of Air Cooled Axial Flux Permanent Magnet Machines" Imperial College London PhD Thesis, March 2010.
[34] http://www.adapted-solutions.com
[35] M. El-Refaie, J. P. Alexander, S. Galioto, P. Reddy, K-K. Huh, P. de Bock, X. Shen, "Advanced High Power-Density Interior Permanent Magnet Motor for Traction Applications," IEEE Energy Conversion Congress and Exposition, 2013, ECCE'13, pp. 581 - 590.
[36] J. Goss, D. Staton, R. Wrobel, P. Mellor, "Brushless AC Interior-Permanent Magnet Motor Design: Comparison of Slot/Pole Combinations and Distributed Vs. Concentrated Windings," IEEE Energy Conversion Congress and Exposition, 2013, ECCE'13, pp. 1213 - 1219.
[37] Wrobel R., Goss J., Mlot A., Mellor P., "Design Considerations of a Brushless Open-Slot Radial-Flux PM Hub Motor," *IEEE Transactions on Industry Applications*, (*early access paper*).
[38] G. Vainel, D. A. Staton, F. G. Capponi, G. De Donato, F. Caricchi, "Thermal Modelling of a Fractional-Slot Concentrated-Winding Kaman Type Axial-Flux Permanent-Magnet Machine," IEEE Energy Conversion Congress and Exposition, 2013, ECCE'13, pp. 1505 - 1511.
[39] D. A. Howey, "Thermal design of air-cooled axial flux permanent magnet machines," *Doctoral Thesis*, *Imperial College London*, UK, 10 March 2010.
[40] www.skf.com (SKF Bearing Calculator)
[41] J. Kunz, C. Siwei, D. Yao, J. R. Mayor, R. G. Harley, T. G. Habetler, "Design of a 750,000rpm Switched Reluctance Motor For Micro Machining," *Energy Conversion Congress and Exposition, (ECCE 2010)*, pp. 3986-3992, September 2010.
[42] D. Jie, D. Yi, C. Bednar, H. Liles, J. Restrepo, J. R. Mayor, R. Harley, T. Habetler, "Electromagnetic Design Considerations for 50,000rpm 1kW Switched Reluctance Machine Using a Flux Bridge," *International Electric Machines and Drives Conference, (IEMDC 2013)*, pp. 325-331, May 2013.
[43] A. Parviainen, "Design of axial-flux permanent-magnet low-speed machines and performance comparison between radial-flux and axial-flux machines," *Doctoral Thesis, Lappeenranta University of Technology*, Finland, 19 April, 2005.
[44] F. Menter, M. Kuntz and R. Langtry, "Ten Years of Industrial Experience with the SST Turbulence Model," Turbulence, Heat and Mass Transfer 4, Begell House, Inc, 2003.
[45] F. Menter, J. Carregal Ferreira, T. Esch and B. Konno, "The SST Turbulence Model with Improved Wall Treatment for Heat Transfer Predictions in Gas Turbines," Proceedings of the International Gas Turbine Congress Tokyo, November 2-7, 2003